Heterogeneous & Homogeneous & Bio- & Nano-

CHEMCATCHEM

CATALYSIS

Accepted Article

Title: Preparation of Zn3In2S6/TiO2 for enhanced CO2 photocatalytic reduction activity via Z-scheme electron transfer

Authors: Houde She, Yan Wang, Hua Zhou, Yuan Li, Lei Wang, Jingwei Huang, and Qizhao Wang

To be cited as: *ChemCatChem* 10.1002/cctc.201801745

Link to VoR: http://dx.doi.org/10.1002/cctc.201801745

A Journal of ChemPubSoc Europe

WILEY-VCH

www.chemcatchem.org

Preparation of $Zn_3In_2S_6/TiO_2$ for enhanced CO_2 photocatalytic reduction activity via Z-scheme electron transfer

Houde She, Yan Wang, Hua Zhou, Yuan Li, Lei Wang, Jingwei Huang, Qizhao Wang*

Abstract: Photocatalytic reduction of CO_2 is increasingly attracting research interest for the growing concerns about climate change resulted from the greenhouse effect due to the industrial emission of CO_2. In this paper, we report the synthesis of $Zn_3In_2S_6$ modified TiO_2 nanocomposite via a facial hydrothermal method. The samples were characterized by photoluminescence spectra (PL), UV–vis diffuse reflectance spectra (DRS), X-ray diffraction (XRD), scanning electron microscopy (SEM), transmission electron microscope (TEM), X-ray photoelectron spectroscopy (XPS) and energy dispersive X-ray spectroscopy (EDS). The production rate of CO from CO_2 is dramatically improved over the obtained composite catalyst. The contact between $Zn_3In_2S_6$ and TiO_2 is responsible for this ameliorated photocatalytic activity because of the formation of the Z-scheme charge transfer mechanism which favors the separation of photo-induced charges.

Introduction

With a considerable increase in greenhouse gas discharge [1], seeking an environment-friendly way to address the problem generated by redundant carbon dioxide has become an urgent need in today's society. Employing CO_2 as a reactant and chemically preparing expected materials for industrial application is one of the most applicable ways. So far, artificial conversion methods of CO_2 mainly embrace high-temperature catalytic hydrogenation [2], photocatalytic conversion [3], photoelectric cooperative catalysis [4], etc. Many catalysts like metal oxides [5-7], sulfides [8-9] and nonmetallic oxide [10-11] have been developed for the purpose of reduction of CO_2 driven by irradiation of visible light and exhibited excellent performance in catalyzing the reaction.

Since S. Kato and F. Mosuo reported the oxidation of tetralin while using TiO_2 as the photocatalyst in a liquid phase under UV irradiation [12], TiO_2 has been extensively studied because of its impressive chemical stability and low cost. However, TiO_2 shows egregious recombination of photogenerated charges and is exclusively responsive to UV light, restricting its further pragmatic use. Therefore, a list of strategies, such as doping [13-14], loading cocatalyst [15] and forming heterojunction with other semiconductors [16] etc. have been explored to solve the problems. Amid them, loading cocatalyst is an efficacious approach, which is capable of greatly improving the efficiency of photo-generated carriers' separation [17].

Precious metals are often used as cocatalysts in carbon dioxide reduction. Nevertheless, they are prohibited from extensive use owning to their high cost. Accordingly, using non-noble metals and its compound as cocatalysts have been studied in a large scale [18, 19], such as copper oxide [20], Co_3O_4 [21] and MoS_2 [22]. Among them, metal sulfides (CdS, $ZnIn_2S_4$, $Zn_3In_2S_6$, etc.) are visible-light-active photocatalysts with unique electronic structure and optical properties [23-28]. Specifically, Zn-In-S, a visible light responding ternary semiconductor, has drawn widespread attention in photocatalysis owning to its high activity and narrow bandgap [29, 30]. For example, Bai's group used $ZnIn_2S_4$ shells as visible light sensitizers to improve light-harvesting efficiency, and resultantly presents significantly enhanced photoelectrochemical performance [31]. Guang Yang et al. prepared $ZnIn_2S_4/TiO_2$ Z-system to reduce recombination of photogenerated electrons and holes with greatly ameliorated catalytic activity attained [32]. One-unit-cell $ZnIn_2S_4$ layers with rich zinc vacancies were successfully designed by Xingchen Jiao et al. for acquiring higher efficiency in photocatalytic reduction of CO_2 [9]. While many studies aiming at $ZnIn_2S_4$, few are focused on $Zn_3In_2S_6$ that plays the role of cocatalyst in photocatalytic reduction of CO_2. In fact, $Zn_3In_2S_6$ owns suitable conduction band position, which will incur a synergistic effect when interacts with other semiconductor materials [33]. In this regard, adopting $Zn_3In_2S_6$ as a cocatalyst can be a quite promising strategy to enhance the photocatalytic activity of TiO_2.

In this study, a new hybrid photocatalyst, $Zn_3In_2S_6/TiO_2$ (ZIS/TiO_2), was synthesized by the solvothermal method. The practical application of it shows that ZIS/TiO_2 composites have better photocatalytic properties than TiO_2 alone. The reason presumably lies in that the contact between cocatalyst $Zn_3In_2S_6$ and TiO_2 forms a direct Z-scheme electron transfer mechanism, raising the separation efficiency of photo-generated carriers. The photocatalytic reaction mechanism of Z-scheme electron transfer was further elucidated by fluorescence spectroscopy, transmission electron microscopy and theoretical calculations.

Dr. H. She, Y. Wang, H. Zhou, Y. Li, Dr. L. Wang, Dr. J. Huang, Prof. Q. Wang
College of Chemistry and Chemical Engineering
Northwest Normal University
Lanzhou 730070, China
E-mail: wangqizhao@163.com; qizhaosjtu@gmail.com.

10.1002/cctc.201801745

Results and Discussion

Morphological analysis of pure TiO_2 and 0.5ZIS/TiO_2 is performed using the field emission scanning electron microscopy (FE-SEM) and the transmission electron microscope (TEM). Fig. 1a, b show illustrative images of the original TiO_2 and 0.5% $Zn_3In_2S_6$ sample. Compared with original P25, 0.5ZIS/TiO_2 has no obvious changes in particle size and morphology. The possible reasons for this result could be demonstrated as follows: The relatively low temperature was used in the preparation of composite materials, which cannot change the primeval physical properties. On the other hand, it may be due to the low content of $Zn_3In_2S_6$ on TiO_2. The transmission electron microscope pictures of TiO_2 and 0.5ZIS/TiO_2 are shown in Fig. 1c and 1d. Two sets of different lattice images are observed in Fig. 1c. It can be seen that two sets of the corresponding streaks, with a distance of 0.355 nm and 0.226 nm, are in great keep with (101) lattice plane of anatase TiO_2 and (200) lattice plane of rutile TiO_2. There are two sets of diverse lattice images in Fig. 1d. One set of the corresponding fringes, with an interval of 0.351 nm and 0.193 nm, are in perfect accord with (101) lattice plane of anatase TiO_2 and (110) lattice plane of $Zn_3In_2S_6$. The structure of 0.5ZIS/TiO_2 composite can be further confirmed by XRD and EDS analysis (shown in Fig. 2,3.) and selected area electron diffraction (shown in Fig. S2.).

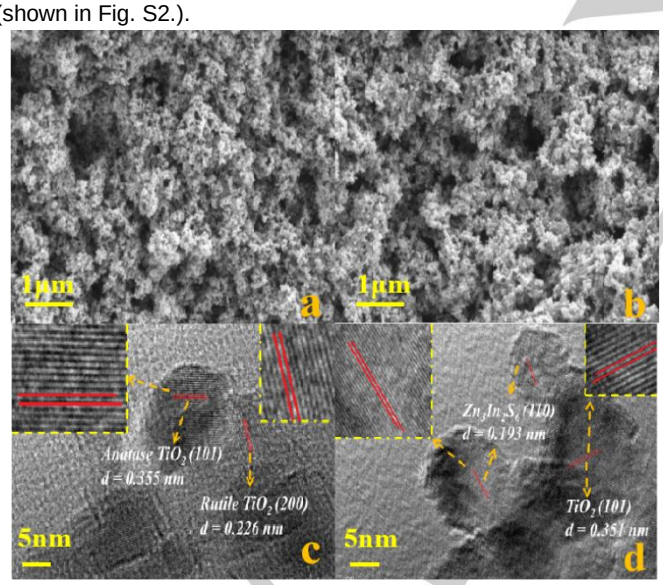

Fig.1 SEM images of (a) TiO_2 and (b) 0.5ZIS/TiO_2; TEM images of (c) TiO_2 and (d) 0.5ZIS/TiO_2.

The X-ray diffraction (XRD) patterns of the as-synthesized pure TiO_2 and TiO_2 with different amounts of $Zn_3In_2S_6$ samples are shown in Fig. 2a. The X-ray peaks of the TiO_2 powder are in fine accordance with rutile phase (JCPDS, No. 21-1276) and anatase phase (JCPDS, No. 21-1272). The X-ray diffraction (XRD) spectrum of the pure $Zn_3In_2S_6$ powder is shown in Fig. 2b, and it is found that the diffraction peak is finally consistent with the JCPDS of the hexagonal phase $Zn_3In_2S_6$, No. 80-0835. Moreover, the diffraction peak intensity of ZIS/TiO_2 gradually decreases with the increase of the loading of $Zn_3In_2S_6$ in the composites. The characteristic peak of $Zn_3In_2S_6$ is not observed because of its low content.

The structure of 0.5ZIS/TiO_2 composite can be further confirmed by EDS analysis as shown in Fig.3. The matching elemental mappings of Ti are feckly uniform with that of O as shown in Fig.3, both of which entirely shape through the TiO_2 substrates structure. Additionally, it can be detected that the equably distributed elemental mappings of Zn, In, S are similar to each other, as suggested by its uniform colour, and no other elements are detected at the same time, which validates the coexistence of $Zn_3In_2S_6$ and TiO_2.

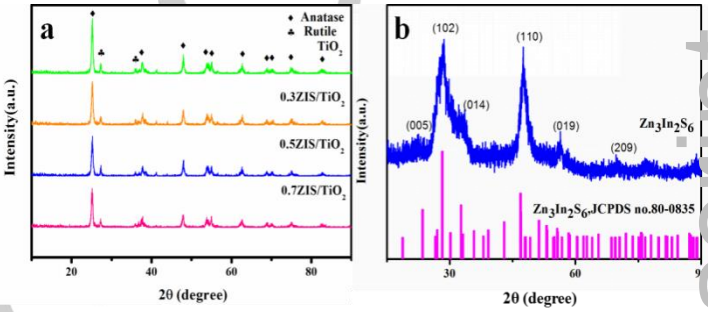

Fig.2 The X-ray diffraction patterns of TiO_2 and ZIS/TiO_2 samples (a) and $Zn_3In_2S_6$ sample (b).

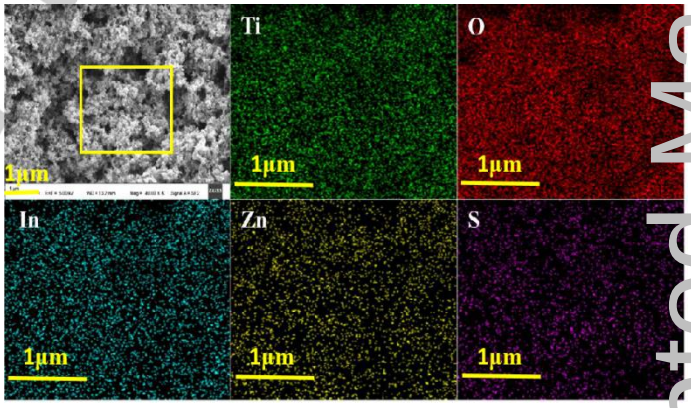

Fig.3 Elemental mapping images of 0.5ZIS/TiO_2

In order to further study the valence state of $Zn_3In_2S_6$ in the composite material, XPS measurements were performed on the as-prepared 0.5ZIS/TiO_2 sample. In Fig. 4a, the Zn 2p core splits into 2p 3/2 and 2p 1/2 peaks at 1021.70 eV and 1044.72 eV, which are consistent with the values for Zn^{2+} [34, 35]. Fig. 4b shows the energy spectrum of In 3d, and there are two peaks located at 444.8 eV and 452.4 eV, which correspond to the binding energy of In 3d 5/2 and In 3d 3/2, respectively. It proved that the valence state of element In is +3 [36, 37]. The XPS spectrum of S 2p in Fig. 4c can be divided into two peaks observed at 161.4 eV and 162.8 eV, which belong to S 2p3/2 and S 2p1/2, indicating the valence of S is -2 [38, 39].

Fig. 5a shows UV–vis diffuse reflectance spectra (DRS) of the TiO_2, 0.3ZIS/TiO_2, 0.5ZIS/TiO_2, 0.7ZIS/TiO_2 and $Zn_3In_2S_6$. As shown in Fig.5a, TiO_2 possesses the strongest absorption in the ultraviolet region, and the absorption wavelength is around 385

10.1002/cctc.201801745

nm. Fig. 5b shows that the band gap of pure TiO_2 is 3.22 eV, which agrees well with the reported value [40, 41]. The strongest absorption peak of $Zn_3In_2S_6$ lies in the visible light region as shown in Fig.5a. The band gap of $Zn_3In_2S_6$ is 2.39 eV as shown in the inserted digital photo of Fig.5b. Compared with pure TiO_2, the introduction of $Zn_3In_2S_6$ has few effects on the absorption of TiO_2 in the UV region. The absorption edge of ZIS/TiO_2 exhibits a valid redshift into the visible light region. The band gap of ZIS/TiO_2 is smaller than that of TiO_2, which is probably due to the subsequently formed energy level after the contact of ZIS and TiO_2 as well as overlap and bending of the bands between $Zn_3In_2S_6$ and TiO_2.

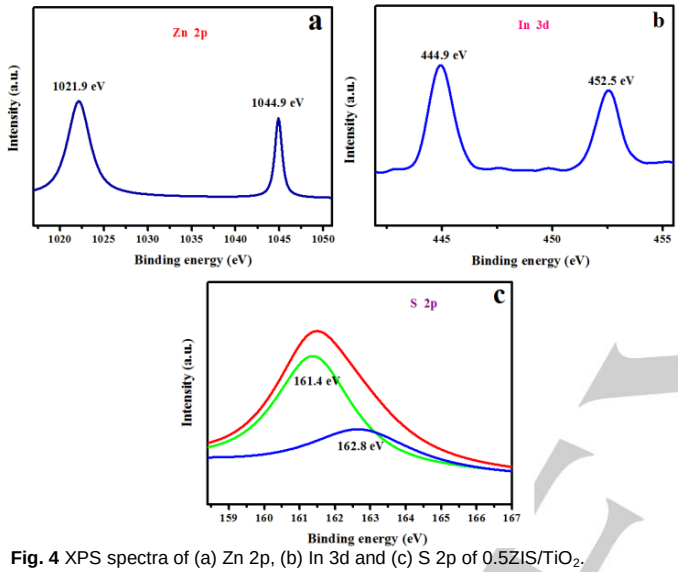

Fig. 4 XPS spectra of (a) Zn 2p, (b) In 3d and (c) S 2p of 0.5ZIS/TiO_2.

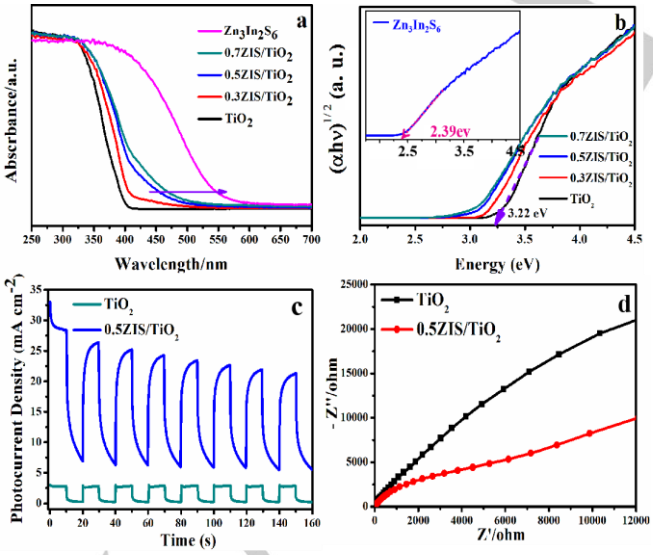

Fig.5 (a) UV–vis diffuses reflectance spectrum and (b) the optical absorption edges of the TiO_2 and ZIS/TiO_2 samples; the inserted digital photo is the optical absorption edges of $Zn_3In_2S_6$. (c) I-t curves of pure TiO_2 and 0.5ZIS/TiO_2 photo-electrodes at 0.8 V vs. REH bias potential in 0.5 M Na_2SO_4 (pH ~ 7.35). (d) Nyquist plots of EIS measurements on the pure TiO_2 and 0.5ZIS/TiO_2 at the open circuit potential in 0.5 M Na_2SO_4 (pH ~ 7.35).

In order to further understand the mechanism in CO_2 photocatalytic reduction catalyzed by ZIS/TiO_2, photoelectrochemical (PEC) properties of TiO_2 and ZIS/TiO_2 were measured. Fig. 5c shows the I-t curves of pureTiO_2 and ZIS/TiO_2. ZIS/TiO_2 presents ideal photocurrents intensity rather than TiO_2. This trend is ascribed to the chummy interfacial links between $Zn_3In_2S_6$ and TiO_2, which promote interfacial charge transfer and enhance separation efficiency of photo-generated carriers. These photocurrent results suggest that $Zn_3In_2S_6$ can efficaciously generate photo-induced electrons in ZIS/TiO_2 and effectively reduce the odds of recombination [42]. This result is also consistent with the test results of the CO_2 photocatalytic reduction performance under 300W Xe lamp. The electrochemical impedance spectroscopy (EIS) can further probe into the separation efficiency of photo-induced electron-hole pairs and present the transfer resistance across the solid-liquid junction in the electrode-electrolyte interface region [43, 44]. The Nyquist plots of TiO_2 and 0.5ZIS/TiO_2 are shown in Fig.5d. At the same high frequency, TiO_2 and 0.5ZIS/TiO_2 show one arc each while the arc of ZIS/TiO_2 suddenly decreased at low frequency, indicating $Zn_3In_2S_6$/TiO_2 possesses the greater separation efficiency of electron-hole and the faster charge transfer on interface [9].

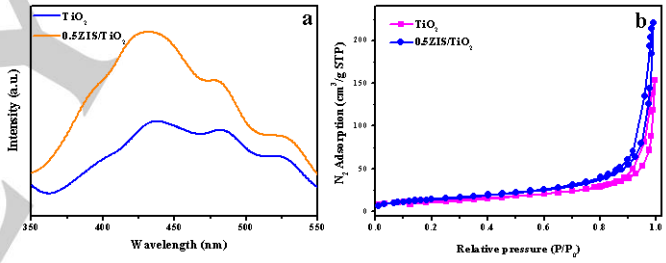

Fig. 6 (a) PL spectra and (b) the N2 adsorption-desorption isotherm of TiO2 and 0.5ZIS/TiO_2.

Fig. 6a displays photoluminescence (PL) spectra of both pure TiO_2 and 0.5ZIS/TiO_2 hybrid photocatalysts. Obviously, the emission intensity of 0.5ZIS/TiO_2 photocatalyst is higher than that of pristine TiO_2. This phenomenon can be explained by the presence of the more photoexcited charge carriers as well as the reduced recombination rate in the photocatalytic system of ZIS/TiO_2 in comparison to neat TiO_2. Commonly, the fluorescence intensity of photocatalyst is lowered because electrons are transferred to the surface of the cocatalyst which suppresses the photocarriers' recombination rate. However, in this study, the fluorescence intensity of the composite material is so apparently enhanced, which is not able to be appropriately explained by the aforementioned theory. In this regard, it is proposed that the composite material transfers electrons through a Z-scheme electron transfer process, suggesting that in the photocatalytic reaction, photogenerated electrons from conduction band (CB) of TiO_2 and photo-induced holes from valence band (VB) of $Zn_3In_2S_6$ recombined at the interface between TiO_2 and $Zn_3In_2S_6$, and thus facilitated the valid charge separation on both CB of $Zn_3In_2S_6$ and VB of TiO_2.

To further understand the nano-porous structures of TiO_2 and 0.5ZIS/TiO_2, the N_2 adsorption-desorption isotherm was performed (Fig. 6b). The test results show that the specific

surface area of pure TiO_2 is 44.79 $m^2 \cdot g^{-1}$, whereas 0.5ZIS/TiO_2 has a higher specific surface area of 51 $m^2 \cdot g^{-1}$. A large specific surface area is beneficial for a catalyst to provide more active sites for the photocatalytic reaction. This result is consistent with the photocatalytic performance test results.

The consequences for CO_2 photocatalytic conversion of the different samples are shown in Fig. 7a. It can be clearly seen that the rates of photocatalytic reduction of CO_2 into CH_4 are 0.2 μmol/(h·g) for TiO_2, 4.75 μmol/(h·g) for 0.3ZIS/TiO_2, 6.19 μmol/(h·g) for 0.5ZIS/TiO_2, 3.815 μmol/(h·g) for 0.7ZIS/TiO_2 and 0.18 μmol/(h·g) for $Zn_3In_2S_6$. Also, their photocatalytic reduction rates of transforming CO_2 into CO are 0.15 μmol/(h·g), 12.93 μmol/(h·g), 23.35 μmol/(h·g), 8.73 μmol/(h·g) and 0.9 μmol/(h·g), respectively. These results indicate that the photocatalytic reduction rate of photocatalyst gradually rises along with the increment in the $Zn_3In_2S_6$ content. The composite material exhibits the best photocatalytic performance when 0.5% $Zn_3In_2S_6$ was loaded on the composite. The absorption edge is broadened and the charge separation efficiency is enhanced at the interface between TiO_2 and $Zn_3In_2S_6$ via a Z-scheme route, which is responsible for the high photocatalytic activity of ZIS/TiO_2. Whereas, when $Zn_3In_2S_6$ was loaded up to 0.7%, the photocatalytic activity decreased. The CB electrons of TiO_2 cannot be excited by light when the redundant $Zn_3In_2S_6$ cover over TiO_2, leading to less photo-generated electrons produced from TiO_2 to consume the photo-generated holes of $Zn_3In_2S_6$. It eventually results in falling of charge carriers' separation efficiency and lower redox ability of photocatalyst. The photocatalytic performance cycle test is shown in Fig.7b, demonstrating a stable recycling performance of 0.5ZIS/TiO_2. The XRD results of the samples after cycling further confirms its stability, as shown in Figure 7c.

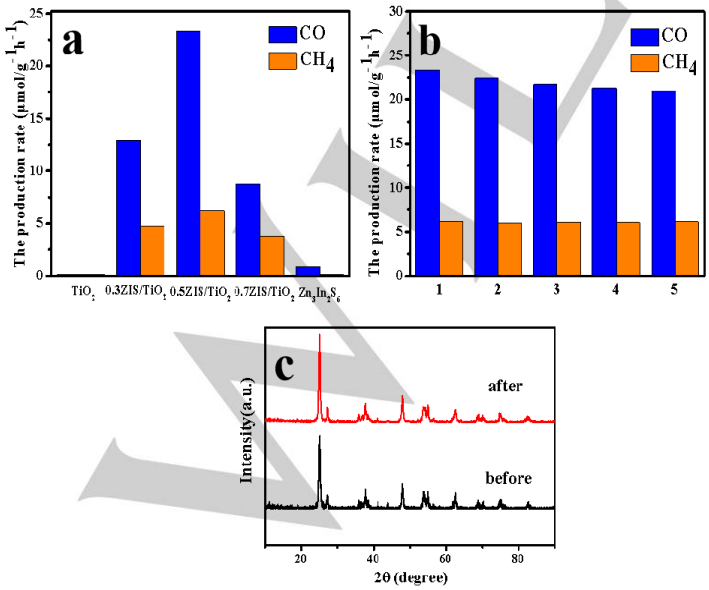

Fig.7 (a) CO and CH_4 generation velocity over TiO_2, 0.3ZIS/TiO_2, 0.5ZIS/TiO_2, 0.7ZIS/TiO_2 and $Zn_3In_2S_6$ under 300 W Xe lamps; (b) Cycling runs in the photocatalytic CO_2 conversion of 0.5ZIS/TiO_2 under 300 W Xe lamps; (c) XRD patterns of 0.5ZIS/TiO_2 sample before and after recycling.

To further investigate the fundamental mechanism of photocatalytic CO_2 conversion, the conduction and valence band edge positions of $Zn_3In_2S_6$ and TiO_2 are calculated from the absolute electronegativity values via following empirical formula [45]:

$E_{VB} = X - E + 0.5\ E_g$(1)

$E_{CB} = E_{VB} - E_g$ (2)

E_{VB}, E_{CB}, E, E_g and X are valence band edge potential, conduction band edge potential, the free electron energy on hydrogen scale with energy of 4.5 eV, band gap and the geometric mean of electronegativity of the constituent atoms forming the semiconductor materials, respectively. The electronegativity of the constituent atoms are X_{Ti} = 3.45, X_O = 7.54, X_{Zn} = 4.45, X_{In} = 3.1, and X_S = 6.22 [46]. The calculated electronegativity of TiO_2 is 5.81 eV, and the electronegativity of $Zn_3In_2S_6$ is 5 eV. The ECB and EVB of TiO_2 and $Zn_3In_2S_6$ are calculated by equations (1) and (2), the valence band positions for TiO_2 and $Zn_3In_2S_6$ are found to be at 2.92 eV and 1.7 eV, with their conduction band positions at -0.3 eV and -0.69 eV.

The potentials for reducing CO_2 relative to the normal hydrogen electrode in water are shown in equations 1 and 2 (pH=7) [47], in which the protons come from the photocatalytic water splitting.

$CO_2 + 2H^+ + 2e^- \rightarrow CO + H_2O$, E^0_{redox} = -0.53 eV (1)

$CO_2 + 8H^+ + 8e^- \rightarrow CH_4 + H_2O$, E^0_{redox} = -0.24 eV (2)

$2H_2O + 4h^+ \rightarrow 4H^+ + O_2$, E^0_{redox} = 0.82 eV (3)

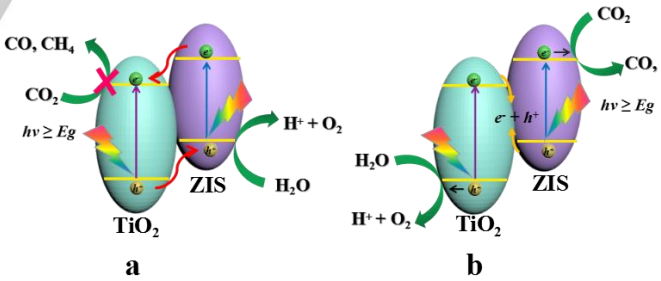

Fig.8 The CO_2 photocatalytic reduction error mechanism of ZIS/TiO_2 (a) and the CO_2 photocatalytic reduction right mechanism of ZIS/TiO_2.

According to the suitable band gap structures and Fermi level [48-51] of TiO_2 and $Zn_3In_2S_6$, the possible transfer processes of photogenerated electron-hole pairs are proposed in Fig. 8. One possible explanation of the photo-generated carrier transfer process is presented in Fig. 8a. The photogenerated electrons in the CB of $Zn_3In_2S_6$ migrate to the CB of TiO_2 while the photoexcited holes in the VB of TiO_2transfer to the VB of $Zn_3In_2S_6$. Subsequently, the ECB of the photogenerated electrons is -0.3 eV. Because the E0 redox(CO_2/CO) is -0.53 eV, CO_2 cannot be reduced to CO. Thereby, the presumed process in Fig. 8a is not feasible in this photocatalysis.

Another possible reaction mechanism is shown in Fig. 8b. In the photocatalytic reaction, the solid-solid contact interface

between $Zn_3In_2S_6$ and TiO_2 serves as the combination center of the photogenerated electrons in the CB of TiO_2 and the photogenerated holes in the VB of $Zn_3In_2S_6$ [40], resulting in an increased fluorescence [42]. The photogenerated electrons involved in the reaction have a stronger reduction ability than that of pure TiO_2, and thus perform a better photocatalytic activity for CO_2 reduction [32]. The photogenerated holes in the VB of TiO_2 oxidize water to form H^+ and O_2, while the photogenerated electrons in the CB of $Zn_3In_2S_6$ simultaneously reduce CO_2 to generate CO or CH_4. In summary, all of the above analyses show that the electron transfer process of ZIS/TiO_2 is identified as Z-scheme electron transfer in this study.

Conclusions

In summary, $Zn_3In_2S_6$/TiO_2 as a new hybrid photocatalyst was successfully prepared by a simple hydrothermal method. 0.5%ZIS/TiO_2 was found to exhibit best photocatalytic activity and excellent stability in CO_2 reduction under simulated solar light irradiation. The most likely reaction mechanism is the Z-scheme electron transfer in this study, which was demonstrated by the photoluminescence (PL) measurements and the results of the photocatalytic CO_2 reduction. The band gap edge of $Zn_3In_2S_6$ can match with TiO_2 well, which provides a promising route for improving CO_2 photocatalytic reduction efficiency. The ZIS/TiO_2 composites have a strong photocatalytic activity because of the higher electron-hole separation efficiency and the stronger reduction ability than TiO_2.

Experimental Section

Certain amount of (0.3%, 0.5%, 0.7%) $Zn(NO_3)_2{\cdot}6H_2O$ and $In(NO_3)_3{\cdot}4.5H_2O$ were dissolved in 54 ml ethylene glycol under constant magnetic stirring to form a solution, to which 0.3 g P25 was added and magnetically stirred for 0.5 h, followed by 1 h ultrasonic oscillation to obtain a suspension, to which certain amount of thioacetamide was added under magnetic stirring for 0.5 h. The mixed solution was poured into a 100 mL Teflon vessel held in a stainless steel autoclave and was maintained at 140 °C for 12 h. After that, the system was cooled down to room temperature. The obtained yellow suspension was washed by water and ethanol several times, and then completely dried in an oven at 60 °C for 24 h. The molar ratio of Zn, In and thioacetamide was kept at 1: 2: 8, and the molar ratio of Zn and TiO_2 was 0.3%, 0.5%, 0.7% for different samples which were labeled as 0.3ZIS/TiO_2, 0.5ZIS/TiO_2, and 0.7ZIS/TiO_2, respectively.

0.5 mmol $Zn(NO_3)_2{\cdot}6H_2O$ and 1 mmol $In(NO_3)_3{\cdot}4.5H_2O$ were dissolved in 54 ml ethylene glycol under constant magnetic stirring for 0.5 h. Subsequently, 4 mmol thioacetamide was added to above solution under constant magnetic stirring for 0.5 h. The following steps are the same as the synthesis of $Zn_3In_2S_6$/TiO_2 except that no P25 was added during the experiment.

Supporting Information Summary

All the information about the testing methods of materials is presented in the Supporting Information.

Acknowledgements

This work is financially supported by the National Natural Science Foundation of China (21663027, 21808189), the Program for the Young Innovative Talents of Longyuan and the Program for Innovative Research Team (NWNU-LKQN-15-2).

Keywords:

Cocatalyst, CO_2 photocatalytic reduction, TiO_2, $Zn_3In_2S_6$, Z-scheme electron transfer

1 L. Wang, S. Duan, P. Jin, H. She, J. Huang, Z. Lei, T. Zhang and Q. Wang, Appl. Catal., B, **2018,** 239, 599-608.
2 C. S. Chen, W. H. Cheng, S. S. Lin, *Appl. Catal.*, A, **2003**, 238, 55-67.
3 S. Sato, T. Morikawa, T. Kajino, and O. Ishitani, *Angew. Chem.*, **2013**, 125, 1022-1026.
4 X. Chang, T. Wang, P. Zhang, Y. Wei, J. Zhao, and J. Gong, *Angew. Chem.*, **2016**, 128, 8986 -8991.
5 T. N. Huan, P. Simon, A. Benayad, L. Guetaz, V. Artero, and M. Fontecave, *Chem. Eur. J.*, **2016**, 22, 14029-14035.
6 M. Karamad, H. A. Hansen, J. Rossmeisl, and J. K. Nørskov, *ACS Catal.*, **2015**, 5, 4075-4081.
7 Y. Pan, Y. You, S. Xin, Y. Li, G. Fu, Z. Cui, Y. Men, F. Cao, S. Yu, and J. B. Goodenough, *J. Am. Chem. Soc.*, **2017**, 139, 4123−4129.
8 A. Aljabour, D. Hazar Apaydin, H. Coskun, F. Ozel, M. Ersoz, P. Stadler, N. S. Sariciftci, and M. Kus, *ACS Appl. Mater. Interfaces*, **2016**, 8, 31695-31701.
9 X. Jiao, Z. Chen, X. Li, Y. Sun, S. Gao, W. Yan,C. Wang, Q. Zhang, Y. Lin, Y. Luo, and Y.Xie, *J. Am. Chem. Soc.*, **2017**, 139, 7586−759.
10 J. Jin, J. Yu, D. Guo, C. Cui, and W. Ho, *Small*, **2015**, 11, 5262-5271.
11 J. Low, J.Yu, and W. Ho, *J. Phys. Chem. Lett.*, **2015**, 6, 4244-4251.
12 K. Kato, F. Masuo, *Kogyo Kagaku Zashi*, **1964**, 67(8), 1136–1140.
13 H. She, H. Zhou, L. Li, L. Wang, J. Huang and Q. Wang. *ACS Sustain. Chem. Eng,* **2018**, 6, 11939-11948.
14 Z. Xiong, Z. Lei, S. Ma, X. Chen, B. Gong, Y. Zhao, J. Zhang, C. Zheng, J. C.S. Wu, *Appl. Catal., B*, **2017,** 219, 412–424.
15 L. L. Tan, W. J. Ong, S. P. Chai, A. R. Mohamed, *Appl. Catal., B*, **2015**, 166-167, 251-259.
16 C. Wang, R. L. Thompson, J. Baltrus, and C. Matranga, *J. Phys. Chem. Lett.*, **2010**, 1, 48-53.
17 Z. Xiong, Z. Lei, C. C. Kuang, X. Chen, B. Gong, Y. Zhao, J. Zhang, C. Zheng, J. C.S. Wu, *Appl. Catal., B* , **2017,** 202, 695-703.
18 Q. Wang, T. Niu, L. Wang, C. Yan, J. Huang, J. He, H. She, B. Su and Y. Bi, *Chem. Eng. J*, **2018**, 337, 506-514.
19 Q. Wang, J. He, Y. Shi, S. Zhang, T. Niu, H. She, Y. Bi and Z. Lei, *Appl. Catal. B,* **2017**, 214, 158-167.
20 L. Tan, Y. Yang, N. Li, S. Chen, Z. Liu, *Catal. Sci. Technol*, **2017**, 7, 1315-1323.
21 D. S. Lee, H. J. Chen, Y. W. Chen, *J. Phys. Chem. Solids*, **2012,** 73, 661-669.
22 W. Tu, Y. Li, L. Kuai, Y. Zhou, Q. Xu, H. Li, X. Wang, M. Xiao and Z. Zou, *Nanoscale*, **2017**, 9, 9065-9070.
23 R. Wei, Z. Huang, G. Gu, Z. Wang, L. Zeng, Y. Chen, Z. Liu, *Appl. Catal. B Environ*, **2018**, 231, 101-107.

24 K. Iwashina, A. Iwase, Y. H. Ng, R. Amal, A. Kudo, *J. Am. Chem. Soc.,* **2015**, 137, 604-607.
25 J. Han, *Z. Liu*, K. Guo, B. Wang, X. Zhang, T. Hong. Applied Catalysis B: Environmental, **2015**, 163: 179-188.
26 W. Chen, Y. X. Hua, Y. Wang, T. Huang, T. Y. Liu, X. H. Liu, *J. Catal.*, **2017**, 349, 8.
27 S. K. Batabyal, S. E. Lu, J.J. Vittal, *Cryst. Growth Des.* **2016**, 16, 2231.
28 A. Iwase, S. Yoshino, T. Takayama, Y. H. Ng, R. Amal, A. Kudo, *J. Am. Chem. Soc.,* **2016**, 138, 10260.
29 J. Song, C. Ma, W. Zhang, S. Yang, S. Wang, L. Lv, L. Zhu, R. Xia, X. Xu, *J. Mater. Chem. B*, **2016**, 4, 7909-7918.
30 B. Xu, P. He, H. Liu, P. Wang, G. Zhou, and X. Wang, *Angew. Chem.,* **2014**, 126, 2371-2375.
31 Z. Bai, X. Yan, Z. Kang, Y. Hu, X. Zhang, Y. Zhang, *Nano Energy* , **2015**, 14, 392-400.
32 G. Yang, D. Chen, H. Ding, J. Feng, J. Z. Zhang, Y. Zhu, S. Hamid, D. W. Bahnemann, *Appl. Catal., B,* **2017**, 219, 611-618.
33 J. Zhang, S. Meng, X. Ye, C. Ling, S. Zhang, X. Fu, S. Chen, *Appl. Catal., B,* **2017**, 218, 420-429.
34 Q. Liu, H. Lu, Z. Shi, F. Wu, J. Guo, K. Deng, and L. Li, *ACS Appl. Mater. Interfaces,* **2014**, 6(19), 17200-17207.
35 X. Wang, S. Li, Y. Ma, H. Yu, J. Yu, *J. Phys. Chem. C,* **2011**, 115(30), 14648-14655.
36 C. Tan, G. Zhu, M. Hojamberdiev, K. S. Lokesh, X. Luo, L. Jin, J. Zhou, P. Liu, *J. Hazard. Mater.* **2014,** 278, 572-583.
37 L. Yuan, M. Yang, Y. Xu, *J. Mater. Chem. A,* **2014,** 2(35), 14401-14412.
38 Zhang C, Xu Y J. *ACS Appl. Mater. Interfaces,* **2013**, 5(24), 13353-13363.
39 H. Yu, W. Liu, X. Wang, F. Wang, *Appl. Catal. B-Environ,* **2018**, 225, 415-423.
40 J. Pascual, J. Camassel, and H. Mathieu, *Phys. Rev. Lett.,* **1977**, 39, 1490-1493.
41 H. Yu, P. Xiao, J. Tian, F. Wang, J. Yu, ACS Appl. Mater. Interfaces, **2016**, 8, 29470-29477.
42 R. Ye, H. Fang, Y. Zheng, N. Li, Y. Wang, and X. Tao, *ACS Appl. Mater. Interfaces,* **2016,** 8, 13879-13889.
43 N. Li, G. Liu, C. Zhen, F. Li, L. Zhang, H. Cheng, *Adv. Funct. Mater.,* **2011**, 21, 1717-1722.
44 Z. Hosseini, N. Taghavinia, N. Sharifi, M. Chavoshi, M. Rahman, *J. Phys.Chem. C,* **2008,** 112, 18686–18689.
45 Y. Xu and M.A.A. Schoonen , *Am. Mineral.,* 2000, 85, 543-556.
46 D. C. Ghosh, T. Chakraborty, *J. Mol. Struct. Theochem,* **2009,** 906, 87-93.
47 Y. Pan, Y. You, S. Xin, Y. Li, G. Fu, Z. Cui, Y. Men, F. Cao, S. Yu, and J. B. Goodenough, *J. Am. Chem. Soc.,* **2017**, 139, 4123-4129.
48 Z. Huang, J. Song, X. Wang, L. Pan, K. Li, X. Zhang, L. Wang, J. Zou, *Nano Energy,* **2017,** 40, 308-316.
49 I. Poulios and N. Papadpoulos, *Solar Energy Materials,* **1990**, 20, 43-51.
50 V. Subramanian, E. E. Wolf, and P. V. Kamat, *J. Am. Chem. Soc.,* **2004**, 126, 4943-4950.
51 P. Zhou, J. Yu, and M. Jaroniec, *Adv. Mater.,* **2014,** 26, 4920-4935.
52 G. Zhou, M. Wu, Q. Xing, F. Li, H. Liu, X. Luo, J. Zou, J. Luo, A. Zhang, *Appl. Catal. B-Environ,* **2018**, 220, 607–614.

10.1002/cctc.201801745

Entry for the Table of Contents

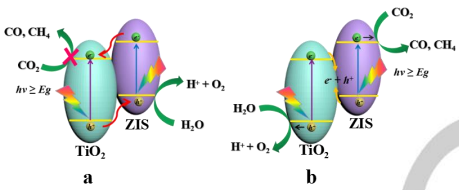

Zn3In2S6 was used to modify TiO2 based photocatalytic system, giving rise to a greatly improved reduction of CO2 into CO. The ameliorated photocatalytic activity might be ascribable to Z-scheme electron transfer, resulting in dramatically enhanced separation and transfer efficiencies of photo-induced electron-hole.